59TH ANNUAL CONFERENCE ON

MAGNETISM AND MAGNETIC MATERIALS

3-7 NOVEMBER 2014 • HONOLULU, HAWAII

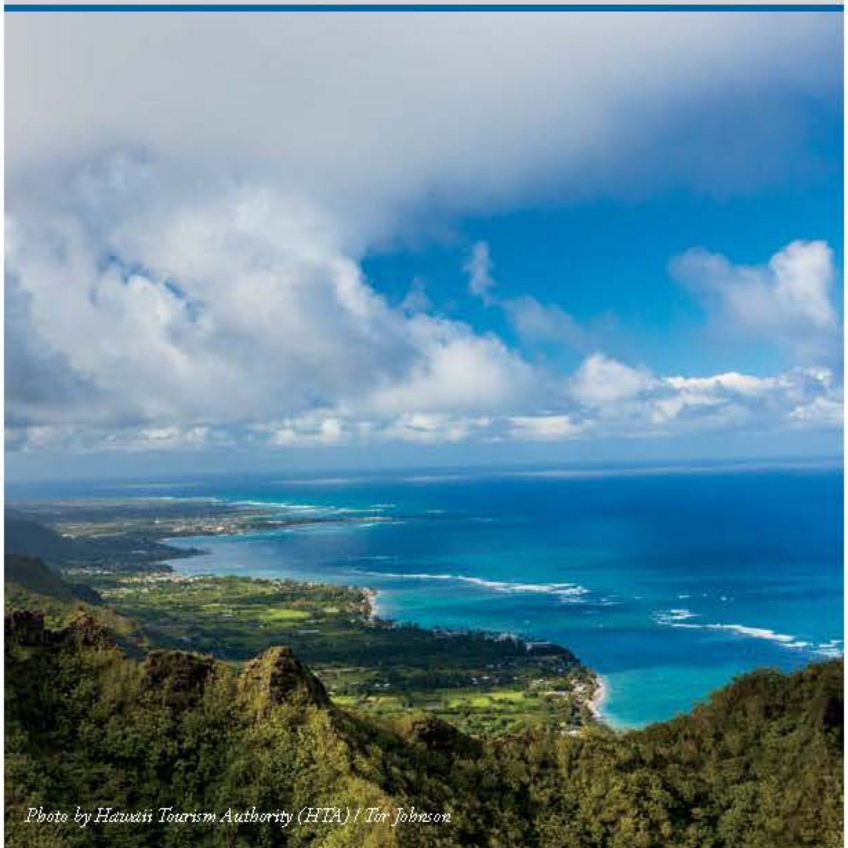

Photo by Hawaii Tourism Authority (HTA) / Tor Johnson

PROGRAM

MMM 2014 Honolulu

AIP Publishing

IEEE MAGNETICS 50 YEARS 1964 2014

Jointly sponsored by AIP Publishing, LLC and the IEEE Magnetics Society

GU-16. Magnetic anisotropy and magnetic moment of tetragonal distorted FeCo films on $L1_0$ FePt underlayer. *B. Wang*[1], H. Oomiya[1], A. Arakawa[1], T. Hasegawa[1], H. Sasaki[1] and S. Ishio[1] *1. Department of Materials Science and Engineering, Akita University, Akita, Akita, Japan*

FRIDAY
MORNING
9:30

CORAL LOUNGE (POSTERS)

Session GV
POWER AND CONTROL MAGNETICS (Poster Session)
Ziyao Zhou, Chair

GV-01. Magneto-resistive Sensor for Nondestructive Testing of Rotor Blade Tips. *E. Cardelli*[1], A. Faba[1], R. Marsili[1], G. Rossi[1] and R. Tomassini[1] *1. Ingegneria, Universita di Perugia, Perugia, Italy*

GV-02. A crawling and drilling microrobot driven by an external precessional magnetic field. S. Kim[1], *G. Jang*[1], S. Jeon[1] and J. Nam[1] *1. Dept of Mechanical Convergence Engineering, Hanyang University, Seoul, Republic of Korea*

GV-03. Multiple-Receptor Wireless Power Transfer for Magnetic Sensors Charging on Mars via Magnetic Resonant Coupling. *C. Liu*[1], K. Chau[1], Z. Zhang[1] and C. Qiu[1] *1. Department of Electrical and Electronic Engineering, The University of Hong Kong, Hong Kong, China*

GV-04. An Orientated Approach for Wireless Charging System in Electric Vehicle Application . *F. Lin*[1], K.T. Chau[1] and C. Liu[1] *1. Department of Electrical and Electronic Engineering, The University of Hong Kong, Hong Kong, Hong Kong*

GV-05. Determination of Ferrite Magnet Shape Considering Magnetization Process. *K. Kim*[1], J. Lee[2], S. Chai[1] and J. Hong[1] *1. Automotive engineering, Hanyang Univ., Seoul, Republic of Korea; 2. KETI, Bucheon, Republic of Korea*

GV-06. Study on Magnetic Flux Cancellation Phenomena in Multiple-transmitter Wireless Charging System. *C. Qiu*[1], K. Chau[1], C. Liu[1] and Z. Zhang[1] *1. The University of Hong Kong, Hong Kong, Hong Kong*

GV-07. Optimization of a thermomagnetic motor. *V. Franzitta*[1], G. Cipriani[1], V. Di Dio[1], F. Raimondi[1] and A. Viola[1] *1. DEIM, University of Palermo, Palermo, Italy*

Paper Number: GV-05

Examination of Ferrite Magnet Shape Considering Magnetization Process

K.S. Kim[1], J.J. Lee[2], S.H. Chai[1], and J. P. Hong[1*]

[1]Department of Automotive Engineering, Hanyang University, Seoul 133-791, Korea

[2]Department of Intelligent Mechatronics Research, Korea Electronics Technology Institute, Bucheon-si 420-733, Korea

*Corresponding Author

Abstract

This paper deals with the post-assembly magnetization process of motors using ferrite permanent magnets. In order to meet the needs of mass production, most motors are magnetized post-assembly. However, increasingly complex shapes are required to maximize the flux of permanent magnets. As a result, certain locations in the magnet are not fully magnetized by the magnetizing fixture due to insufficient magnetomotive force. Therefore, an analysis concerning the post-assembly magnetization is needed. In this paper, the concentrated flux spoke type synchronous motor is analyzed to magnetization process, and then the magnetization level is compared by linkage flux value between post-assembly and fully magnetization. Finally, back electromotive force is estimated by post-assembly magnetization method the according to the magnet shape.

.

1. Introduction

Recently, environmental issues have worsened, and the depletion of fossil fuels has accelerated. To alleviate these problems, motors with much higher efficiency are required [1-3]. Electric motors have been used in household appliances and industrial power sources since shortly after their development, and the implementation of motors expanded to vehicle and mechanical systems thereafter.

Since its development, various aspects of the motor have been studied in an effort to meet the specific needs of the motor's operator: for example, efficiency, power density, cost of operation, etc. One particular type of motor, the interior permanent magnet synchronous motor (IPMSM), is widely used to meet the demand of high power density, with rare earth permanent magnets (PM) frequently being essentially incorporated [4].

However, the rare earth permanent magnet is both costly and sparse. The rarity of the PM subsequently generates imbalances in supply and increases in price. Therefore, new types of motor have been proposed to eliminate the need for rare earth materials, without sacrificing performance. For example, there are axial gap type machines, wound rotor type machines, induction machines, IPMSMs that utilize ferrite magnets, etc. Concentrated flux spoke type motors, using ferrite PMs, are particularly attractive. In this type of motor, in order to increase the flux of the ferrite magnet, the magnet's shape and arrangement become increasingly complex. For obtaining the motor performance as designed, magnet quality must be guaranteed. In the mass production system, the post assembly magnetization method is used. As a result, certain locations in the magnet are not fully magnetized. Therefore, magnet shape and arrangement are the important factors [5], [6].

In this paper, the post-assembly magnetization method is analyzed with respect to the concentrated flux spoke type motor. According to this process, the non-magnetized PMs are installed on the v-shaped rotor. The rotor and stator are combined after discharging current flows into the magnetizing fixture and rotor with PM. According to the magnet shape, the back EMF is calculated by finite element method (FEM).

2. PM performance according to magnetic field intensity

The PMs can be either isotropic or anisotropic, depending on the production method. Generally speaking, the residual flux density of anisotropic PMs is higher than that of isotropic PMs. In the anisotropic PM, the hard axis along a non-preferred direction is assumed to be linear. The preferred direction shows the nonlinear performance in the easy axis. The PM materials along the easy axis have a nonlinear B-H curve as shown in Fig. 1. In the magnetizing force H=0 and flux density B=0, this is the initial point of the non-magnetized magnet. During the magnetization process, when H increases, B will increase along the initial magnetization curve. At this time, when H decreases, B will decrease along the demagnetization curve. When H=0, this flux density is the residual flux density. If H is increased in the reverse direction form B=Br to B=0, the H point of B=0 is called the coercive force. If H is not sufficient, B cannot reach the saturation point. Therefore, when H=0, Br is lower than fully saturated. Additionally, during this time, coercive force drops and recoil permeability grows. All of these various effects ultimately influence the motor's performance. Therefore, during the post-assembly magnetization procedure, proper magnet shape and arrangement provide for sufficient magnetic field intensity.

3. Post-assembly magnetization process

In mass production, productivity is influenced by product state which may be complexity, material, and etc. Therefore, in the motor design consider the productivity. The magnet's shape is an important factor that is related to the motor's performance. In this paper, magnetization level and back EMF are studied in post- assembly magnetization according to the PM shape. Fig.2 shows the post-assembly magnetization process.

3.1 Calculation of discharging current

For magnetizing the PMs, a magnetizing fixture is needed. The magnetizing fixture is combined with a condenser bank that supplies sufficient voltage [7], [8]. Fig. 3 shows the magnetizing fixture circuit with the condenser bank. If the switch is turned on, discharging current flows into the magnetizing fixture, which is combined with the rotor. The diode prevents current from flowing counter-clockwise. The circuit is governed by the following system of equations:

$$L\frac{d^2i(t)}{dt^2}+R\frac{di(t)}{dt}+\frac{1}{C}i(t)=0 \quad (1)$$

$$i(0)=0 \quad (2)$$

$$\frac{di(0)}{dt}=\frac{V_0}{L} \quad (3)$$

where L=L_p+L_m, L_p is the parasite inductance, L_m is inductance of the magnetizing fixture with rotor, R=R_p+R_m, R_p is the parasite resistance, R_m is the resistance of the magnetizing fixture, C is the capacitance of the condenser bank, $i(t)$ is the current flowing into the magnetizing fixture, and V_0 is the initial voltage on the capacitor. L is calculated by magnitude according to the discharging current. Equations (2) and (3) are the initial conditions for solving the differential equation (1).

MATLAB SIMULINK is used to solve the differential equation (1). Fig. 4 shows the block diagram of the differential equation of magnetizing fixture circuit. The input values are R, L, C, V_0, while the output value is the current $i(t)$. Fig.5 shows the discharging current, which results from differential equation (1).

3.2 PM magnetization

For analyzing the PM magnetization using FEM, discharging current and material data (which are covered with the PM initial magnetization curve) are needed. The residual flux density, recoil permeability, and coercive force of the PM element are calculated by the PM's B-H curve after the FEM is conducted.

3.3 Analysis of motor parameter

Using the PM's completed magnetization, the motor parameter will be analyzed by FEM. Occasionally, some element of the PM may generate a lower flux than what would be predicted if it were fully magnetized. Therefore, if the PM is not fully magnetized, the linkage flux or back EMF is lower than what it would otherwise be.

4. Analysis model

The analysis model is based on the compressor motor in an air conditioner. Fig. 6 shows the analysis model, and Table I shows the specification. This motor is the concentrated flux spoke type using ferrite PM. For obtaining the motor flux in the PM, the PM is spoke type of 8 pole and the v-shape. The PM is hexagonally shaped, which maximizes the flux given the limited width. Although sufficient discharging current flows into the magnetizing fixture, the edge of PM (A) may be not fully magnetized. In this paper, the magnetization level is examined with respect to the shape of the PM's edge. Fig.7 shows the FEM modeling of analysis model. The post-assembly magnetization analysis is conducted by simulation according to this paper chap.3.

5. Results

Fig. 8 shows residual flux density according to element number. The flux density of the rectangular magnet (a) is distributed to 0.447 T, which is the fully magnetized level. However, the flux density of the hexagonal magnet (b) ranges from 0 to 0.447 T. Table II shows the mean and standard deviation concerning tow case. The standard deviation of model (b) is larger than model (a). However, the mean value of model (b) is not much lower than model (a), because the magnet area is larger than the edge area.

The back EMF and magnetization level are shown in Fig. 9. The magnetization level is calculated by post-assembly magnetization divided by full magnetization. The level of model (a) is 99.93%, model (b) is 95.32%. The magnetization level of model (b) result from the edge which is not fully magnetized. Although the model (b) is not fully magnetized, the model (b) of back EMF is higher than the model (a).

4. Conclusions

In this paper, the magnetization level of PM is studied by examining the effects of the magnetizing fixture in post-assembly magnetization. Because PM is not fully magnetized in post-assembly magnetization, magnetization analysis is needed. In order to increase flux, sufficient PM edge area is needed, and the concentrated flux spoke type motor provides this. Accordingly, this study applies to motors that incorporate magnets with complex shapes.

Acknowledgments

This research was supported by the MSIP (Ministry of Science, ICT, and Future Planning), Korea, under the C-ITRC (Convergence Information Technology Research Center) support program (NIPA-2013-H0401-13-1008) supervised by the NIPA (National IT Industry Promotion Agency).

References

[1] C.Breton, *et al*., *IEEE Trans. Magn.*, Vol. 36, No. 5, pp. 3819-3823 (2000)

[2] Z. Q. Zhu, *et al*., *IEEE Trans. Magn.*, Vol. 39, No. 5, pp. 3238-3240 (2003)

3 B. H. Lee, *et al.*, *IEEE Trans. Magn.*, Vol. 48, No. 11, pp. 2949-2952 (2012)

[4] J. Hur and B.W. Kim, *JEET* Vol. 5, No. 3, pp. 462-467 (2010)

[5] D. G. Dorrell, *et al*., *IEEE Trans. Magn.*, Vol. 43, No. 6, pp. 2489-2491 (2007)

[6] C. K. Lee, B. I. Kwon, *IEEE Trans. Magn.*, Vol. 41, No. 5, pp. 1928-1931 (2005)

[7] J. Kelly Lee, *et al*., *J. Appl. phys*., Vol. 67, No. 3, pp. 1570-1575(1990)

[8] S. L. Ho, *et al*., *IEEE Trans. Magn.*, Vol. 48, No. 11, pp. 3238-3241 (2012)

List of Tables:

TABLE I
SPECIFICATIONS OF THE ANALYSIS MOTOR

	Unit	Value
Phase / poles / slots	-	3 / 8 / 12
Outer radius of stator	mm	100
Outer radius of rotor	mm	100
Max torque	Nm	2.4
Input voltage	Vrms	220
Current limit	Arms	15
Outer diameter	mm	100
Br (fully magnetization)	T	0.41
Thickness of PM	mm	4

TABLE II
MEAN AND STANDARD DEVIATION

	Model (a)	Model (b)
PM shape	Rectangular	Hexagon
Mean	0.4466	0.4326
Standard deviation	0.0022	0.0418

List of Figures

FIGURE 8. Residual flux density according to element number: (a) rectangular magnet shape; (b) hexagon magnet shape

FIGURE 9. Residual flux density according to element number: (a) rectangular magnet shape; (b) hexagon magnet shape